www.amlett.com, www.vbripress.com/aml, DOI: 10.5185/amlett.2015.5721 Published online by the VBRI press in 2015

Fabrication and plasmonic characterization of Au nanowires with controlled surface morphology

Ina Schubert[1*], Wilfried Sigle[2], Loic Burr[1,3], Peter A. van Aken[2], Christina Trautmann[1,3], Maria Eugenia Toimil-Molares[1]

[1]*Materials Research Department, GSI Helmholtzzentrum für Schwerionenforschung GmbH, Darmstadt, Germany*
[2]*Stuttgart Center for Electron Microscopy, Max Planck Institute for Intelligent Systems, Stuttgart, Germany*
[3]*Department of Materials and Geo Science, Technische Universität Darmstadt, Darmstadt, Germany*

[*]Corresponding author. Tel: (+49) 6159712033; E-mail: i.schubert@gsi.de

Received: 02 November 2014, Revised: 04 March 2015 and Accepted: 08 March 2015

ABSTRACT

Gold nanowires are attracting great attention due to their ability to sustain surface plasmons and are thus promising candidates for sensing applications such as surface enhanced Raman and infrared spectroscopy. Controlling all nanowire parameters is crucial to adjust the resonance wavelengths and to obtain high electric field enhancements. We have fabricated Au nanowires with controlled dimensions and surface morphology by electro-deposition of Au and Au-Ag nanowires in the pores of ion-track-etched polymer templates. Smooth and rough nanowires are fabricated by the use of different polymer types. By dealloying of Au-Ag wires, porous Au wires are being created. In addition, we have analyzed the surface plasmonic properties of smooth and porous Au nanowires by scanning transmission electron microscopy combined with electron energy-loss spectroscopy. Our results reveal the excitation of five different longitudinal modes in the smooth as well as in the porous Au wire. The resonance energies of the porous wire are red-shifted compared to the energies of a smooth Au wire with same dimensions, which demonstrates that the surface morphology of the nanowire is an important parameter to tune the multipole surface plasmon modes to specific energies. Knowledge on the plasmonic properties of nanowires dependent on their surface morphology is indispensable for their efficient application for sensor technology.

Keywords: Au nanowires; surface plasmons; porosity; STEM-EELS; electro-deposition.

Ina Schubert is Postdoc at the Materials Research Department of GSI Helmholtz Centre for Heavy Ion Research in Darmstadt, Germany. Her research focuses on electrochemical deposition of metal nanostructures in ion-track membranes and surface plasmon investigations.

Introduction

Surface plasmons in metallic nanostructures are currently attracting great attention due to their very high potential for various applications, such as sensor technology **[1-3]**, photo-thermal therapy **[4-6]** and solar cells **[7]**. Surface plasmons are collective electronic oscillations that can lead to very high field enhancements in the nanoparticle near-field. These field enhancements are applied for surface enhanced Raman spectroscopy (SERS) and infrared spectroscopy (SEIRS) to intensify the spectroscopic signals of molecules that are adsorbed on the nanoparticle surface **[8-10]**. For both techniques, fine tuning of the surface plasmon wavelength is crucial. While for SERS it has to be tuned to the Raman laser wavelength, for SEIRS it is adjusted to the molecular vibration wavelength. It is known that the surface plasmon wavelength as well as the field enhancement depends sensitively on various parameters such as the nanostructure dimensions, shape, morphology, and refractive index of the local environment of the nanostructures **[11-13]**. Currently, much effort is devoted to enhancing the sensitivity of the nanostructures by introducing so-called "hotspots" that offer even higher field enhancements than the smooth nanostructure surface. Examples of structures containing efficient hotspots are porous gold films **[14]**, rough Au particles **[8]**, Si wires metallized with Ag particles **[15]**, and metal nanoparticles separated by small gaps **[9, 16-18]**. While for smooth structures SERS enhancement factors of about 10^5 were measured **[19]**, for nanostructures with hotspots enhancement factors up to 10^{11} have been obtained **[9]**. Developing of synthesis methods that allow not only to

adjust the nanostructure dimensions but also to control the surface morphology of the nanostructures is thus beneficial for sensor applications.

For the synthesis of nanostructures, we applied the ion-track technology where nanowires are electro-deposited in ion-track-etched polymer templates **[20]**. The method provides control on a number of nanowire parameters such as length, diameter, geometrical shape, crystallinity, surface morphology, and composition. Cylindrical, conical, and biconical nanostructures have been demonstrated **[20, 21]**. The diameter of the wires can be controlled between 15 nm and several 100 nm, nanowire lengths between 1 µm and 100 µm are possible **[22]**. Recently, rough and smooth $Bi_{1-x}Sb_x$ nanowires were prepared by using different polymer templates **[23]**. A novel approach to further enhance the surface area of the electro-deposited wires and to create voids that may serve as hotspots in plasmonics is the chemical dissolution of the less noble component in alloy wires, which results in the formation of porous structures **[24, 25]**. For spherical porous particles fabricated by a seed-mediated growth process, it has been shown recently that they possess a high plasmonic tunability and enhanced near-fields compared to smooth particles **[26]**.

In this report, we present the electro-deposition of Au nanowires in the pores of ion-track-etched polymer templates using two different approaches to modify (1) the surface roughness and (2) the wire porosity. In addition, the plasmonic properties of smooth and porous Au nanowires are compared using electron energy-loss spectroscopy combined with scanning transmission electron microscopy (STEM-EELS). This method enables us to study the multipole longitudinal and transversal surface plasmons with very high spatial resolution. Our results are crucial for the efficient application of porous nanowires as substrates for SERS and SEIRS.

Experimental

Materials

As templates for the nanowires served 30 µm polycarbonate membranes (Makrofol M) and 12 µm thin polyethyleneterphtalate (PET), both purchased from Bayer. For nanowire electrodeposition two different electrolytes were used. Sulfide-based Au electrolyte with pH-value of 7.5 was obtained from METAKEM (Usingen, Germany) For preparation of cyanide based electrolytes, $KAu(CN)_2$, and Na_2CO_3 were purchased from Carl Roth (Karlsruhe, Germany) and $KAg(CN)_2$ from Sigma Aldrich and dissolved in deionized water. Their concentrations in the different electrolytes are given in the results and discussion section. Si wafers (Si-Mat, Kaufering, Germany) were applied as substrates for scanning electron microscopy (SEM), while 30 nm-thin Si_3N_4 membranes (Plano, Wetzlar, Germany) served as substrates for STEM-EELS. HNO_3 (65%), Dichloromethane (≥99.5%) and NaOH (≥98%) were purchased from Carl Roth.

Method

Au nanowires with controlled surface morphology are fabricated by electro-deposition in ion-track-etched polymer templates. Different polymer foils are irradiated with swift heavy ions at the linear accelerator UNILAC at GSI Helmholtz Centre for Heavy Ion Research in Darmstadt, Germany. Each ion creates along its trajectory a track in the foil consisting of complex damage of the polymer. Subsequent chemical etching of the irradiated polymer using 6 M NaOH at 50 °C selectively dissolves the ion tracks creating nanochannels. The etching time controls the nanochannel diameter. After the etching process, a thin Au film is sputtered on one side of the polymer foil to serve as the cathode for the electro-deposition process. First, the Au film is electrochemically reinforced by a copper layer to completely close the pores and ensure mechanical stability. In a second step, Au or Au-Ag nanowires are electrochemically deposited in the pores of the template. To release the nanowires from the template, the polymer is dissolved using dichloromethane. Afterwards, the nanowires were released from their back-layer by ultrasonification in clean dichloromethane solution. Several of the nanowires were drop-cast on Si wafers or Si_3N_4 membranes.

STEM-EELS measurements were performed at the Zeiss SESAM transmission electron microscope operated at 200 kV at the Max Planck Institute for Intelligent Systems in Stuttgart, Germany. The very high energy resolution of 0.1 eV is obtained by the use of a field-emission gun and an electrostatic omega-type monochromator **[27]**. The present experiments were carried out using a width of 0.12 eV in order to increase the electron probe current and improve the counting statistics. In all spectra that are shown in the following, we have subtracted the zero-loss peak by fitting a power-law function to the positive energy-loss tail of this peak.

SEM analysis of the wires was performed in a Jeol JSM7401-F field emission SEM. Compositional analysis was carried out at 20 kV using a Bruker energy-dispersive X-ray (EDX) detector.

Results and discussion

Fig. 1a and **1b** show Au nanowires obtained from a sulfide-based Au electrolyte (METAKEM, pH 7.5) in a two-electrode arrangement at 50°C with a Au wire as anode. Using different kinds of polymer templates allows us to control successfully the surface morphology of our wires. **Fig. 1a** shows smooth nanowires deposited in a 30 µm thin polycarbonate membrane by applying a voltage of -0.7 V. Rough Au nanowires are created in a 12 µm thin PET foil at a potential of -0.8 V (**Fig. 1b)**.

We have also synthesized Au-Ag alloy nanowires by electrochemical deposition from an electrolyte containing 50 mM $KAu(CN)_2$, 50 mM $KAg(CN)_2$ and 0.25 M Na_2CO_3 in a three-electrode arrangement at 60 °C. A platinum wire served as anode. **Fig. 2a** and **2c** show SEM images of Au-Ag nanowires deposited at voltages of -1.1 V and -0.5 V vs. Ag/AgCl reference electrode, respectively. EDX in SEM measurements of bundles of these nanowires reveal that the created nanowires consist of Ag:Au ratios of about 60:40 and 90:10, respectively. The Si wafers with the wires were dipped into concentrated nitric acid for 3 h to dissolve the Ag in the alloy nanowires and create porous wires. **Fig. 2b** and **2d** show the same nanowires as in **Fig. 2a** and **2c** after the nitric acid treatment. The insets depict parts of the wires at higher magnification. For the wire deposited at higher

voltage (**Fig. 2b**), we observe that it has maintained its overall cylindrical shape and its diameter, but reveals almost homogeneously distributed pores. EDX measurements show that small Ag concentrations of 5-10 at. % remain in the porous nanowires after the nitric acid treatment. Erlenbacher *et al.* have shown in their theoretical work that during dealloying of Au-Ag films the porosity is created by dissolution of Ag atoms on the film surface, along with surface diffusion of the Au atoms **[28, 29]**. The Ag dissolution process proceeds until the complete surface is passivated by Au atoms. Residual Ag atoms may be enclosed by the Au atoms dependent on the initial Au-Ag concentration. High-resolution transmission electron microscopy (HRTEM) analysis for a deeper understanding of the dealloying process in our Au-Ag nanowires is in progress and will be reported in a separate manuscript **[30]**.

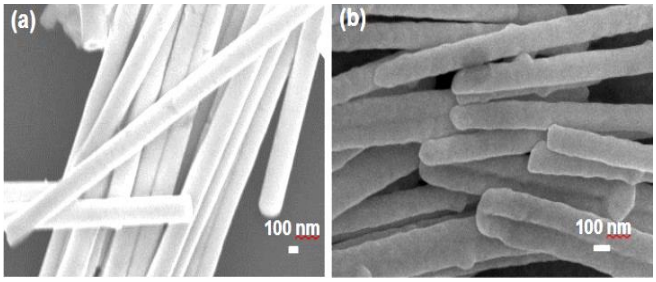

Fig. 1. (a) Smooth Au nanowires with diameter of ~220 nm deposited in polycarbonate and (b) rough Au wires of ~ 140 nm diameter deposited in PET.

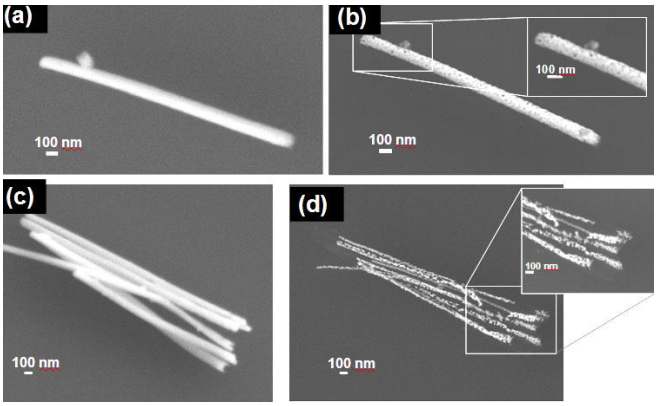

Fig. 2. SEM images of Au-Ag nanowire with Ag:Au composition of 60:40 (a) before and (b) after nitric acid treatment. SEM images of Au-Ag nanowires with Ag:Au ratio of 90:10 (c) before and (d) after nitric acid treatment. The two insets in (b) and (d) show parts of the porous wires at higher magnification.

For the wires fabricated at low voltage (**Fig. 2d**), the structures have even higher porosity and are partly separated into segments. The diameter is strongly reduced compared to the initial wires. This result shows that the initial composition of the nanowire influences strongly the resulting shape and porosity after dealloying. Fine-tuning of the initial Au-Ag concentration is necessary, to adjust the porous structures for special applications. For nanowires with higher Au concentration of 60 %, we find that the wires remain non-porous after the nitric-acid treatment.

The plasmonic properties of our smooth and porous Au nanowires with length of about 1 µm were analyzed by STEM-EELS. It is well known that the electron beam in the TEM excites surface plasmons in Au wires **[31, 32]**. The resonance energies, which depend on the excitation position, are probed by measuring EEL spectra. Positions of high energy-loss probability along the nanowires can be assigned to the positions of the surface charge maxima of the different surface plasmon modes **[33-35]**. First, we discuss the result for a smooth Au wire and secondly we analyse a porous wire with very similar dimensions as the smooth one. Finally, the results are compared to finite element simulations.

Fig. 3a shows a map of 100 STEM-EEL spectra measured along a pure Au nanowire with length L = 895 ± 5 nm and diameter D = 95 ± 5 nm. The wire is deposited from an electrolyte containing 0.25 M Na_2CO_3 and 50 mM $KAu(CN)_2$ at -1.1 V vs. Ag/AgCl electrode. The electron beam is scanned along the wire as indicated by the red arrow in the TEM image. The average distance of the scan line to the nanowire is ~10 nm. Each horizontal line in the map corresponds to one EEL spectrum. The color indicates the energy-loss probability. **Fig. 3b** shows one example spectrum that has been extracted from the map at the position of the red dot in the TEM image on the right. The map reveals the energies for the first five different multipole longitudinal surface plasmon modes together with a broad transversal resonance at 2.3 eV. This transversal mode can be excited at all positions along the wire which distinguishes this mode from all the longitudinal modes. The surface charge distribution for each of the modes is schematically shown on top of the map. For the five longitudinal modes, it is obvious that the energy difference between two consecutive modes as well as the intensity of the maxima decreases with increasing energy. This effect has been previously observed for Au wires of different aspect ratios **[34]**.

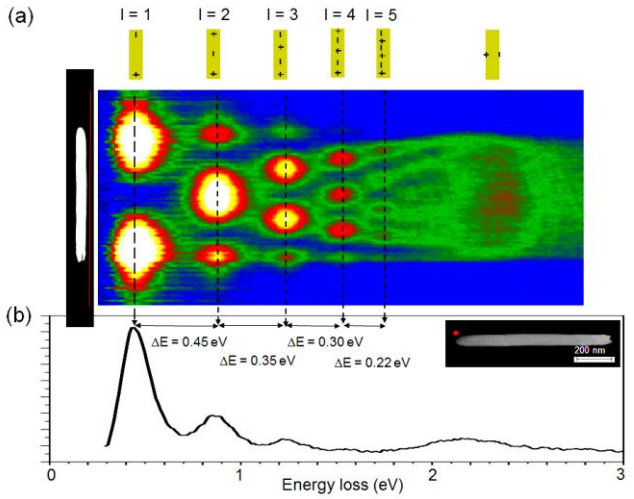

Fig. 3. (a) High-resolution EELS map of a single Au nanowire (L = 895 ± 5 nm and D = 95 ± 5 nm). The electron beam is scanned along the red arrow in the TEM image. The schematics on top of the map illustrate the surface charge distributions for the different surface-plasmon modes and (b) EEL spectrum extracted from the map at the position of the red dot in the TEM image on the right.

In addition, porous nanowires were investigated and the spectra were compared to the ones of the smooth wires. **Fig. 4** shows a TEM image of a typical porous nanowire with line profiles of Ag-L_α and Au-L_α X-ray intensities measured in an SEM along the green arrow. The nanowire

was prepared from an electrolyte containing 50 mM $KAu(CN)_2$ and 50 mM $KAg(CN)_2$ at -1.1 V. The nanowire has a length L = 1000 ± 10 nm and a diameter D = 90 ± 10 nm. The TEM image reveals an inhomogeneous porosity along the wire. The EDX scan allows the distinction of three different parts: A less porous part on the left side, where the Ag concentration is highest; a strongly porous part in the middle of the wire, with pore sizes up to ~20 nm and a lower Ag content; finally a small part on the right which is not porous; here the Ag concentration is lowest. The non-constant Ag concentration has to be considered for the surface plasmon analysis and is caused by the synthesis process. Probably, the Au-rich part is due to the sputtering process during the nanowire synthesis. (To create a cathode for the electro-deposition, a Au layer was sputtered on the backside of the polymer template). It is known that during this process sputtered Au enters the pores, resulting in a short Au nanowire segment. The inhomogeneous porosity is assigned to the hydrophobicity of the Si_3N_4 substrate. A high porosity is related to an efficient dealloying process and thus a resulting small Ag content.

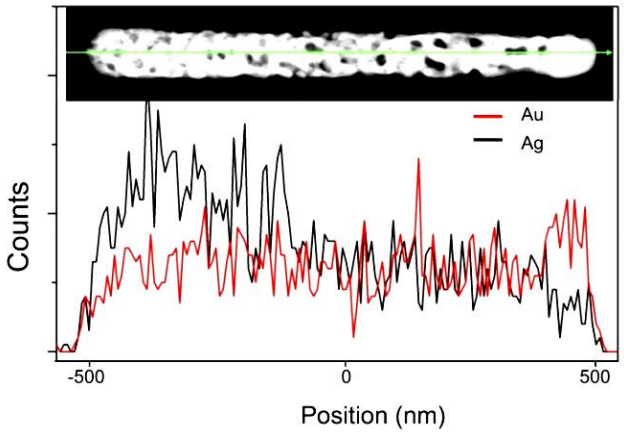

Fig. 4. TEM image of a porous Au nanowire together with line profiles of Ag-L_α (black) and Au-L_α (red) X-ray intensities measured in a SEM.

Fig. 5a shows the high-resolution plasmonic energy-loss map, consisting of 100 EEL spectra, measured along this porous nanowire. As for the pure Au wire, each horizontal line corresponds to one spectrum and the color in the map indicates the number of counts. **Fig. 5b** depicts one spectrum extracted from the map, its acquisition site being marked in the TEM image by the red dot. Similarly as for the pure Au nanowire, the map reveals five low-energy modes that can be assigned to the longitudinal modes of multipole orders l = 1 to 5. Furthermore, the decrease in intensity with increasing energy, and the continuously decreasing energy difference between two consecutive modes can be confirmed also for the porous nanowire. Overall, the porosity of the nanowire seems to have a surprisingly small impact on these five low-order longitudinal surface plasmon modes. As for the pure Au wire, these low-order longitudinal modes reveal in position and intensity almost mirror symmetry to the wire center. On the other hand, for the modes at energies higher than 1.6 eV the symmetry is lost. Several intensity maxima are visible that are shifted in energy depending of the position along the wire and it is difficult to assign them to a specific mode. We assign this to both, the influence of the varying porosity along the nanowire together with the varying Au-Ag composition. We tentatively assign these intensity maxima to transversal modes. From the map in **Fig. 5a** their energies are determined to vary between 1.9 and 2.3 eV and depend on the position along the wire. These energies are lower than the energy of the transversal mode of the pure Au wire centered at 2.3 eV.

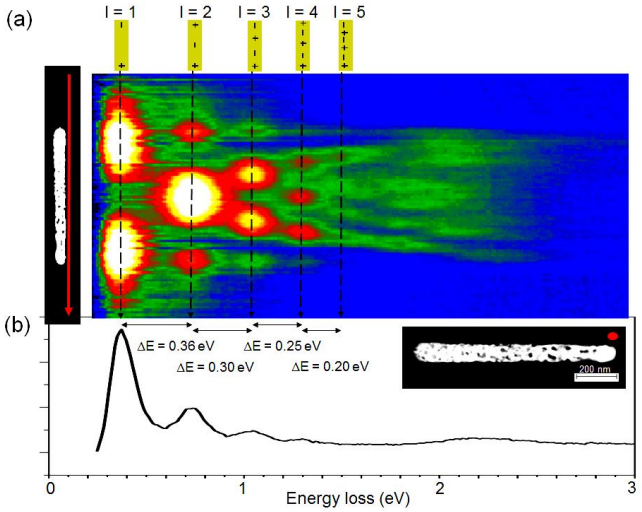

Fig. 5. (a) High-resolution EELS map of a porous Au nanowire with L = 1000 ± 10 nm and D = 90 ± 10 nm. The electron beam is scanned along the red arrow in the TEM image. The schematics reveal the surface charge distributions for the different surface plasmon modes and (b) EEL spectrum extracted from the map at the position of the red dot in the TEM image.

Finally, we have simulated by finite element simulations with CST Microwave Studio the longitudinal multipole-order resonance energies of two single Au nanowires with lengths and diameters identical to the two here experimentally analyzed wires. In our simulations, the surface plasmons are excited by a small radiating dipole located at one end of the nanowire and the electric field strength at the opposite end was calculated. The resonance energies are chosen as the energies where the electric field strength has its maximum. Details on the simulation are described in **[35]**. The nanowires are defined as cylindrical objects with hemispherically shaped edges. The dispersion curve of Au is taken from reference **[36]**. **Fig. 6** shows the resonance energies calculated in the simulation for a Au wire with L = 895 nm, D = 95 nm (red squares) and a Au wire with L = 1000 nm and D = 90 nm (blue squares). In addition, the figure shows the experimentally determined energies for the two wires. For the pure Au wire, there is an obvious red-shift for the experimental determined energies compared to the simulated ones. A comparable red-shift between experiment and theory has been previously reported by other authors **[32, 37]** and originates most probably from uncertainties in the dispersion relation for Au, the surface roughness of the wire, and the shape of the wire ends. For the wire with length L = 1000 nm, we find a much stronger red-shift between the experimental data (porous Au wire) and simulated values (smooth Au wire). This strong red-shift shows that like the transversal mode, also the longitudinal resonance energies of the porous wire are red-shifted compared to the resonance energy of a smooth Au wire with same dimensions. A descriptive

explanation for this red-shift is the increased surface area of the porous wire that results in an intrinsically longer surface plasmon wavelength. This red-shift of the modes of the porous wire is in agreement with the observations reported in reference **[38]** where extinction spectra of short (few hundred nanometers long) porous nanorods were investigated. The authors report that the modes are red-shifted with increasing porosity.

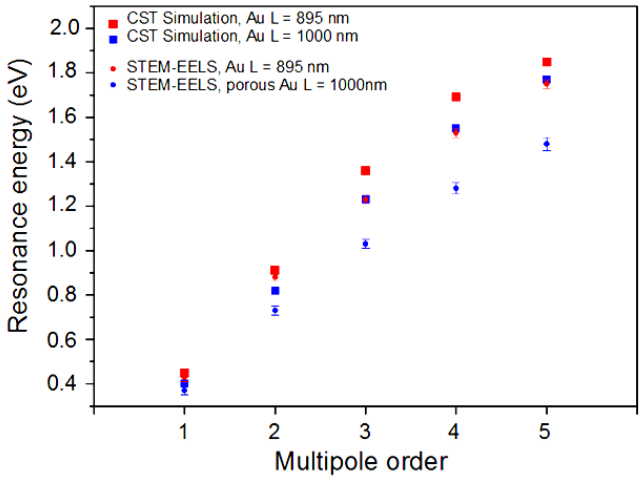

Fig. 6. Surface plasmon resonance energies for the five different multipole modes of the simulated and measured wires. The red squares correspond the simulated values for a Au wire with L = 985 nm and D = 95 nm, the red dots correspond the STEM-EELS results for the wire with corresponding dimensions. The blue squares show the calculated resonance energies for a pure Au wire with L= 1000 nm and D = 90 nm. The blue dots give the data for the STEM-EELS analysis of the porous Au wire with these dimensions.

Conclusion

In conclusion, Au nanowires with controlled surface morphology are created by electro-deposition in ion-track-etched polymer templates and are ideal model systems to test plasmonic properties of nanowires. Our method allows the fabrication of smooth, rough, and porous nanowires. The presented results highlight the potential of the porous Au wires with their increased surface areas and formation of voids as promising Raman substrates. Tuning of the initial Au-Ag concentration is necessary to adjust the porosity and wire shape.

Detailed surface plasmon analysis by STEM-EELS on these wires together with simulations reveal a red-shift of the resonances of porous wires compared to smooth wires with same dimensions. Similar characteristics of the multipole surface plasmon modes for porous wires are found compared to smooth wires, such as decreasing mode intensity with increasing energy, and a continuously decreasing energy difference between two consecutive modes. Our results demonstrate that the surface morphology of a nanowire is an additional parameter for tuning the multipole surface plasmon modes to specific wavelengths, which is of high importance for sensing applications.

Acknowledgements
The research leading to these results has received funding from the European Union Seventh Framework Programme [FP7/2007-2013] under grant agreement n°312483 (ESTEEM2).

Reference

1. Anker, J.N.; Hall, W.P.; Lyandres, O.; Shah, N.C.; Zhao, J.; Van Duyne, R.P.; *Nature Mater.* **2008**, *7*, 442. **DOI:** 10.1038/nmat2162
2. Willets, K.A.; Van Duyne, R.P.; *Annu. Rev. Phys. Chem.* **2007**, *58*, 267. **DOI:** 10.1146/annurev.physchem.58.032806.104607
3. Rosman, C.; Prasad, J.; Neiser, A.; Henkel, A.; Edgar, J.; Sönnichsen, C.; *Nano Lett.* **2013,** *13*, 3243. **DOI:** http://dx.doi.org/10.1021/nl401354f
4. El-Sayed, I.H.; Huang, X.; El-Sayed, M.A.; *Cancer Lett.* **2006,** *239*, 129. **DOI:** 10.1016/j.canlet.2005.07.035
5. Huang, X.; El-Sayed, I.H.: Qian, W.; El-Sayed, M.A.; *J. Am. Chem. Soc.* **2006,** *128*, 2115. **DOI:** 10.1021/ja057254a
6. Jain, P.K.; Huang, X.; El-Sayed, I.H.; El-Sayed, M.A.; *Acc. Chem. Res.* **2008**, *41*, 1578. **DOI:** 10.1021/ar7002804
7. Atwater, H.A.; Polman, A.; *Nature Mater.* **2010**, *9*, 205. **DOI:** 10.1038/nmat2629
8. Fang, J.; Du, S.; Lebedkin, S.; Li, Z.; Kruk, R.; Kappes, M.; Hahn, H. *Nano Lett.* **2010**, *10*, 5006. **DOI:** 10.1021/nl103161q
9. Hatab, N.A.; Hsueh, C.H.; Gaddis, A.L.; Retterer, S.T.; Li, J.H.; Eres, G.; Zhang, Z.; Gu, B.; *Nano Lett.* **2010**, *10*, 4952. **DOI:** 10.1021/nl102963g
10. Neubrech, F., Pucci, A.; Cornelius, T. W.; Karim, S.; García-Etxarri, A.; Aizpurua, J.; *Phys. Rev. Lett.* **2008**, *101*, 157403. **DOI:** 10.1103/PhysRevLett.101.157403
11. Jain, P.K.; Lee, K.S.; El-Sayed, I.H.; El-Sayed, M.A.; *J. Phys. Chem. B* **2006**, *110*, 7238. **DOI:** 10.1021/jp057170o
12. Link, S.; El-Sayed, M.A.; *J. Phys. Chem. B* **1999**, *103*, 4212. **DOI:** 10.1021/jp984796o
13. Link, S.; Mohamed, M.B.; El-Sayed, M.A.; *J. Phys. Chem. B* **1999**, *103*, 3073. **DOI:** 10.1021/jp990183f
14. Qian, L.H.; Yan, X.Q.; Fujita, T.; Inoue, A.; Chen, M.W. *Appl. Phys.Lett.* **2007,** *90*, 153120. **DOI:** 10.1063/1.2722199
15. Fang, C.; Agarwal, A.; Widjaja, E.; Garland, M.V.; Wong, S.M.; Linn, L.; Khalid, N.M.; Salim, S.M.; *Chem. Mater.* **2009**, *21*, 354. **DOI:** 10.1021/cm900132j
16. Theiss, J.; Pavaskar, P.; Echternach, P.M.; Muller, R.E.; Cronen, S.B. *Nano Lett.* **2010**, *10*, 2749. **DOI:** 10.1021/nl904170g
17. Li, S.; Pedano, M.L.; Chang, S.H.; Mirkin, C.A. *Nano Lett.* **2010**, *10*, 1722. **DOI:** 10.1021/nl100099g
18. Huck, C.; Neubrech, F.; Vogt, J.; Toma, A.; Gerbert, D.; Katzmann, J.; Härtling, T.; Pucci, A.; *ACS Nano* **2014,** *8*, 4908. **DOI:** 10.1021/nn500903v
19. Félidj, N.; Aubard, J.; Lévi, G.; Krenn, J.R.; Salerno, M.; Schider, G.; Lamprecht, B.; Leitner, A.; Aussenegg, F.R.; *Phys. Rev. B* **2002**, *65*, 075419. **DOI:** 10.1103/PhysRevB.65.075419
20. Toimil-Molares, M.E.; *Beilstein J. Nanotechnol.* **2012,** *3*, 860. **DOI:** 10.3762/bjnano.3.97
21. Dobrev, D.; Vetter, J.; Neumann, R.; Angert, N.; *J. Vac. Sci. Technol. B* **2001,** *19*, 1385. **DOI:** 10.1116/1.1381066
22. Picht, O.; Müller, S.; Alber, I.; Rauber, M.; Lensch-Falk, J.; Medlin, D.L.; Neumann, R.; Toimil-Molares, M.E.; *J. Phys. Chem. C*, **2012**, *116*, 5367. **DOI:** 10.1021/jp210491g
23. Müller, S.; Schötz, C.; Picht, O.; Sigle, W.; Kopold, P.; Rauber, M.; Alber, I.; Neumann, R.; Toimil-Molares, M.E.; *Cryst. Growth, Des.* **2012**, *12*, 615. **DOI:**10.1021/cg200685c
24. Ji, C.; Searson, P.C.; *Appl. Phys. Lett.* **2002**, *81*, 4439. **DOI:** 10.1063/1.1526920
25. Laocharoensuk R.; Sattayasamitsathit S.; Burdick J.; Kanatharana P.; Thavarungkul P.; Wang J.; *ACS Nano* **2007,** *1*, 403. **DOI:** 10.1021/nn700255x

26. Zhang, Q.; Large, N.; Nordlander, P.; Wang, H.; *J. Phys. Chem. Lett*. **2014**, *5*, 370.
DOI: 10.1021/jz402795x
27. Koch, C.T.; Sigle, W.; Höschen, R.; Rühle, M.; Essers, E.; Benner, G.; Matijevic, M.; *Microsc. Microanal.* **2006**, *12*, 506.
DOI: 10.1017/S1431927606060624
28. Erlebacher, J.Aziz, M.J.; Karma, A.; Dimitrov, N.; Sieradzki, K.; *Nature* **2001**, *410*, 450.
DOI: 10.1038/35068529
29. Erlebacher, J.; Seshadri, R.; *MRS Bulletin* **2009**, *34*, 561.
DOI: 10.1557/mrs2009.155
30. Burr, L.; Schubert, I.; Sigle, W.; Trautmann, C.; Toimil-Molares, M.E.; Article in preparation.
31. Garcia de Abajo, F.J.; Kociak, M.; *Phys. Rev. Lett.* **2008**, *100*, 106804.
DOI: 10.1103/PhysRevLett.100.106804
32. Nelayah, J.; Kociak, M.; Stéphan, O.; Garcia de Abajo, F.J.; Tencé, M.; Henrard, L; Taverna, D.; Pastoriza-Santos, I.; Liz-Marzán, L.M.; Colliex, C.; *Nature Phys.* **2007**, *3*, 348.
DOI: 10.1038/nphys575
33. Rossouw, D.; Couillard, M.; Vickery, J: Kumacheva, E.; Botton, G.A.; *Nano Lett.* **2011**, *11*, 1499.
DOI: 10.1021/nl200634w
34. Alber, I.; Sigle, W.; Müller, S.; Neumann, R.; Picht, O.; Rauber, M.; van Aken, P.A.; Toimil-Molares, M.E.; *ACS Nano* **2011**, *5*, 9845.
DOI: 10.1021/nn2035044
35. Alber, I.; Sigle, W.; Demming-Janssen, F.; Neumann, R.; Trautmann, C.; van Aken, P.A.; Toimil-Molares, M.E.; *ACS Nano* **2012**, 6, 9711.
DOI: 10.1021/nn303149p
36. Palik, E.D. (Ed.); Handbook of optical constants of solids; Academic press, **1998**.
37. Dorfmüller, J; Vogelgesang, R.; Weitz, R.T.; Rockstuhl, C.; Etrich, C.: Pertsch, T.; Lederer, F.; Kern, K.; *Nano Lett.* **2010**, *10*, 3596.
DOI: 10.1021/nl900900r
38. Bok, H.-M., Shuford, K.L.; Kim, S.; Kim.S.K.; Park, S.; *Nano Lett*. **2008**, *8*, 2265.
DOI: 10.1021/nl800924r

